A&A, 695, A120 (2025)
https://doi.org/10.1051/0004-6361/202451840

Astronomy & Astrophysics

Exploring the disc-jet scenario in 3C 273 using simultaneous *XMM-Newton* and *NuSTAR* observations

Ashwani Pandey[1,2,3,⋆], Santanu Mondal[4], and Paul J. Wiita[5]

[1] Center for Theoretical Physics, Polish Academy of Sciences, Al.Lotnikov 32/46, PL-02-668 Warsaw, Poland
[2] Department of Physics and Astronomy, University of Utah, Salt Lake City, UT 84112, USA
[3] Key Laboratory for Particle Astrophysics, Institute of High Energy Physics, Chinese Academy of Sciences, 19B Yuquan Road, Beijing 100049, PR China
[4] Indian Institute of Astrophysics, 2nd Block Koramangala, Bangalore 560034, Karnataka, India
[5] Department of Physics, The College of New Jersey, 2000 Pennington Road, Ewing, NJ 08628-0718, USA

Received 9 August 2024 / Accepted 4 February 2025

ABSTRACT

Context. The well-studied active galactic nucleus (AGN) 3C 273 displays characteristics of both jetted-AGNs and Seyfert galaxies, which makes it an excellent source to study the disc-jet connection in AGNs.
Aims. We aim to investigate the disc-jet scenario in 3C 273 using broad-band (0.3–78 keV) X-ray spectra from *XMM-Newton* and *NuSTAR*.
Methods. We used simultaneous *XMM-Newton* and *NuSTAR* observations of 3C 273 carried out between 2012 and 2024. The 0.3–78 keV X-ray spectra were first fitted with a simple power law (PL) and then with the accretion-ejection-based `JeTCAF` model. The `JeTCAF` model accounts for emission from the jet, which extends up to the sonic surface. In this framework, a reflection hump above 10 keV can also arise due to the bulk motion Comptonization of coronal photons by the jet.
Results. We find that the simple PL did not provide a good fit, leaving significant residuals at energies below 1.5 keV. All the spectra were fitted well by the `JeTCAF` model. The weighted-averaged black hole mass of $(7.77 \pm 0.30) \times 10^8\ M_\odot$ obtained from the `JeTCAF` model is comparable with the previous estimates based on reverberation mapping observations and accretion disc models.
Conclusions. The 0.3–78 keV X-ray emission of 3C 273 can be fit by the accretion-ejection-based model in which the corona and the jet on top of it make significant contributions to the X-ray flux. The Doppler boosting factor estimated from the jet flux ranges from 1.6 to 2.2, consistent with the lower limit from the literature.

Key words. accretion, accretion disks – galaxies: active – galaxies: jets – X-rays: individuals: 3C 273

1. Introduction

It is now well established that the nuclei of active galaxies, called active galactic nuclei (AGNs), host supermassive black holes (SMBHs) that actively accrete material through a disc and generate electromagnetic radiation (e.g. Rees 1984). Evidence of highly collimated relativistic outflows, or jets, has been detected in a fraction (∼10−20%) of AGNs, known as jetted-AGNs, using high-resolution radio imaging and multi-wavelength observations (e.g. Blandford et al. 2019). The formation, acceleration, and collimation of these relativistic jets are still not fully understood. Models available in the literature for jet production assume that they originate in the vicinity of the BHs and extract their power mainly from (a) the BH spin (Blandford & Znajek 1977), and/or (b) the accretion disc (Blandford & Payne 1982). Both of these basic models expect a connection between the relativistic jet and the accretion disc. The disc-jet connection in accreting systems is one of the most important unresolved issues in astrophysics and has been the focus of many studies (e.g. Maraschi & Tavecchio 2003; Livio et al. 2003; Sbarrato et al. 2014; Mukherjee et al. 2019).

Active galactic nuclei that have relativistic jets closely aligned to the observer are known as blazars (e.g. Padovani et al. 2017). Based on the equivalent widths (EWs) of emission lines in their optical spectra, Stocke et al. (1991) classified them as flat spectrum radio quasars (FSRQs; $EW_{rest} > 5$ Å) and BL Lacertae objects (BLLs; $EW_{rest} < 5$ Å). The absence of strong emission lines in BLLs could be due to the presence of a radiatively inefficient disc (Ghisellini et al. 2011).

The first identified quasar, 3C 273, is a nearby ($z = 0.158$; Schmidt 1963) highly luminous FSRQ. It is extremely variable across all the electromagnetic (EM) frequencies (e.g. Soldi et al. 2008); however, unlike most other FSRQs, it shows a low (on average < 1%) degree of optical polarization (Valtaoja et al. 1991; Hutsemékers et al. 2018). Due to its high luminosity and proximity, it has been intensively monitored for flux and spectral variability over the entire (that is, from radio to γ rays) EM spectrum (e.g. Xie et al. 1999; Türler et al. 2000; Sambruna et al. 2001; Kataoka et al. 2002; Fan et al. 2009, 2014; Abdo et al. 2010; Kalita et al. 2015; Madsen et al. 2015; Chidiac et al. 2016; Fernandes et al. 2020).

The submillimetre-to-radio emission of 3C 273 is characterized by strong flux variations that are produced by the synchrotron emission of relativistic electrons within the jet (Türler et al. 2000; Soldi et al. 2008). At optical-to-UV frequencies, a bright excess (blue bump) is usually found that can be interpreted as the contribution from two differently variable components: a blue component and a red component

⋆ Corresponding author; ashwanitapan@gmail.com

(Paltani et al. 1998). The blue component, which is mostly variable in the UV, can be attributed to thermal emission from the accretion disc, while the red component, which is significantly variable in the IR, could be due to the jet emission (Soldi et al. 2008).

In the X-ray band, a soft excess is commonly observed in the low energy (below ∼2 keV) spectra of 3C 273, which can be explained by the thermal Comptonization of UV disc photons in a hot corona above the disc (Grandi & Palumbo 2004). A correlation between low-energy X-ray and UV emission has been found in a few observations that support the Comptonization scenario (e.g. Walter & Courvoisier 1992; Kalita et al. 2015). However, such a correlation was not detected in certain studies (e.g. Chernyakova et al. 2007; Soldi et al. 2008) that question this interpretation.

The spectra of such 'jetted' sources can be described using accretion-disc-jet-based models (Wandel & Urry 1991; Zdziarski & Grandi 2001; Grandi & Palumbo 2004; Mondal et al. 2022a; Das & Chatterjee 2023, and references therein), where UV and X-ray emission might come from the vicinity of the accretion disc. These works found the signature of an accretion disc along with the jet in the X-ray spectra of blazars and FSRQs. As 3C 273 is one such candidate, we attempted to further investigate this possibility by fitting simultaneous broad-band X-ray observations from *NuSTAR* and *XMM-Newton* using an accretion-ejection-based two-component advective flow (`TCAF`; Chakrabarti & Titarchuk 1995) model that has been expanded to include jet emission (`JeTCAF`; Mondal & Chakrabarti 2021). The `JeTCAF` model takes into account the radiation mechanisms in the disc, corona, and at the base of the jet or outflows, and the effect of bulk motion by the outflowing jet on the emitted spectra. We note that apart from the base of the jet, the rest of the jet can also contribute to the spectrum. In the present model, the jet is only considered up to the sonic surface. If the inclusion of the rest of the jet does not change the overall spectral shape but only the total flux in X-rays, the present model parameters could fit the contribution from the rest of the jet with some changes in the model normalization. This model has six parameters: (i) The mass of the BH ($M_{\rm BH}$) if it is unknown; (ii) the Keplerian disc accretion rate ($\dot{m}_{\rm d}$); (iii) the sub-Keplerian halo accretion rate ($\dot{m}_{\rm h}$); (iv) the size of the dynamic corona or the location of the shock within the accretion flow ($X_{\rm s}$ in units of $r_S = 2GM_{\rm BH}/c^2$; Chakrabarti 1989); (v) the shock compression ratio (R), which is the velocity drop across the shock, and therefore the jump in density there; and (vi) the ratio of the solid angle subtended by the outflow to the inflow, $f_{\rm col}(\equiv \Theta_o/\Theta_{\rm in})$. The final parameter may depend on the jet properties. However, since we do not know these properties before model fitting, we take it as a user-defined parameter. Since the mass of the BH is also a parameter in this model, we can determine its value from spectral analysis (e.g. Mondal et al. 2022b), as was done using the `TCAF` model fitting within the standard software package, XSPEC (Debnath et al. 2014; Molla et al. 2017). The spectrum of 3C 273 is complex, including disc and power-law components, soft excess, and a reflection signature. The `JeTCAF` model incorporates both the corona to disc and disc to corona photon interceptions to iteratively compute the spectrum with a modified disc temperature similar to `TCAF`. In addition, when Comptonized photons from the corona pass through the jet medium, this produces a Compton hump. The combination of these two processes changes the X-ray spectrum significantly by producing a hump above 10 keV, similar to so-called reflection models. However, the current model does not include emission processes and therefore cannot produce the often-observed iron lines.

The structure of this paper is as follows. In Sect. 2 we describe the observations and data reduction procedure. The results and our discussion of them are presented in Sect. 3. Section 4 presents our conclusions.

2. Observation and data analysis

NuSTAR observed the blazar 3C 273 on 32 occasions between 2012 July 1 and 2024 January 7. In this work, we only selected observations with an exposure time greater than 5 ks. Also, on 2012 July 13, out of the six observations of almost equal exposures (∼6 ks), we only used the observation with the longest exposure time. We were left with a total of 16 observations with an exposure time ranging from 6.23 ks to 243.97 ks that were performed between 2012 July 13 and 2024 January 7. A detailed log of these observations is given in Table A.1.

We downloaded the *NuSTAR* observations of 3C 273 from the HEASARC data archive[1]. We followed the standard procedures[2] to reduce and analyse the *NuSTAR* datasets using HEASOFT version 6.29 and CALDB version 20210427. We first generated the calibrated, cleaned, and screened event files using the *nupipeline* script. The source and background spectra were then extracted from these cleaned event files using the *nuproducts* script. To extract both source and background spectra, we took circular regions with similar radii (30″). The source region was centred at the source position and the background region was on the same focal plane module but away from the source contamination. We rebinned the *NuSTAR* spectra using the `grppha` routine to have at least 25 counts per spectral bin.

Additionally, we searched for 3C 273 data in the *XMM-Newton* data archive. We found ten *XMM-Newton* observations of 3C 273 that were simultaneous to the *NuSTAR* observations, as listed in Table A.1. To reduce the *XMM-Newton* data of 3C 273, we used the Science Analysis System (SAS v. 21.0.0) and followed the standard procedures[3]. We limited our analysis to the data from the European Photon Imaging Camera (EPIC) pn detector, which is the most sensitive and least impacted by pile-up effects. We started by reprocessing the observation data files (ODFs) to generate the calibrated and concatenated EPIC pn event lists. We then filtered out the periods of high background flares. We chose a circular region of 40″ centred on the source to extract the X-ray spectrum. A background spectrum was also extracted using a circular region of a similar radius from a source-free region. We checked all the observations for pileup using the task `epatplot` and corrected the affected observations by removing a region of radius 7.5″ from the core of the source PSF. Finally, we rebinned the X-ray spectra so we had at least 25 counts for each background-subtracted spectral bin.

3. Results and discussion

We first fitted the 0.3–10 keV *XMM-Newton* spectra of 3C 273 using simple power-law (`PL`) models with the Galactic absorption component `TBABS` using XSPEC version v12.11.0. During the fit, we fixed the value of the hydrogen column density to $1.69 \times 10^{20}\,{\rm cm}^{-2}$ for the Galactic absorption (HI4PI Collaboration 2016). The fits were poor, with $\chi^2_r > 10$

[1] https://heasarc.gsfc.nasa.gov/cgi-bin/W3Browse/w3browse.pl
[2] https://heasarc.gsfc.nasa.gov/docs/nustar/analysis/
[3] https://www.cosmos.esa.int/web/xmm-newton/sas

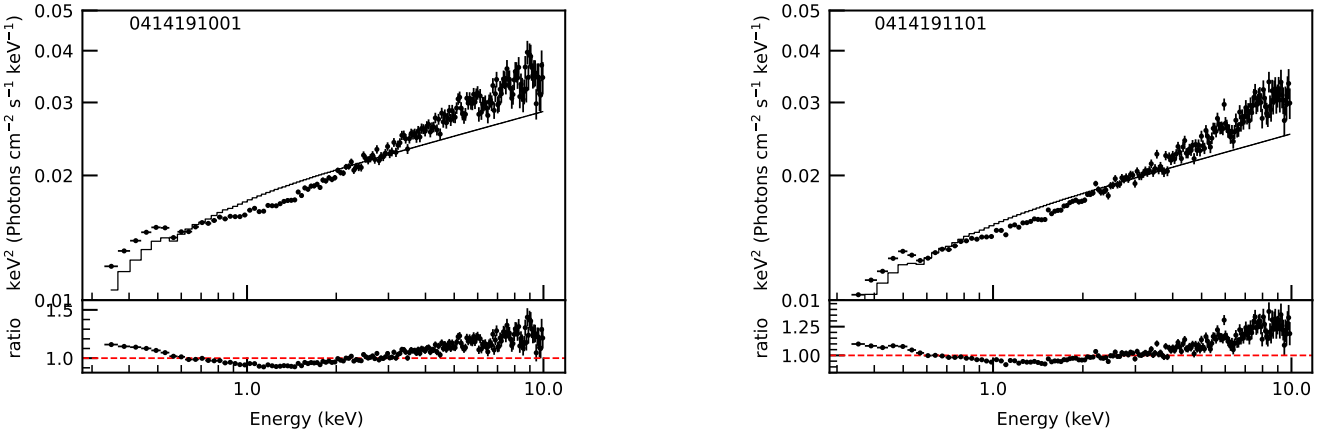

Fig. 1. Sample plots showing TBABS(PL)-fitted 0.3–10 keV spectra of 3C 273 (top panel) and the ratio of data/model (bottom panel). The observation ID is mentioned in each plot. Plots for the remaining *XMM-Newton* observations are shown in Fig. B.1.

Table 1. Best-fitted TBABS(DISKBB+PL) model parameters for all simultaneous *XMM-Newton* and *NuSTAR* observations of 3C 273.

Obs Date	MJD	$T_{\rm in}$ (keV)	$\rm Norm_{diskbb}$	$\Gamma_{\rm PL}$	$\chi^2_{\rm r}$
2012-07-14	56122	0.131 ± 0.003	2996.57 ± 353.90	1.664 ± 0.003	1.10
2015-07-13	57216	0.142 ± 0.004	1467.65 ± 190.93	1.680 ± 0.005	1.22
2016-06-26	57565	0.136 ± 0.003	3228.20 ± 304.37	1.540 ± 0.004	1.57
2017-06-26	57930	0.137 ± 0.003	1409.50 ± 164.90	1.587 ± 0.004	1.25
2018-07-04	58303	0.137 ± 0.003	2646.79 ± 228.69	1.689 ± 0.004	1.37
2019-07-02	58666	0.149 ± 0.003	1700.25 ± 131.37	1.719 ± 0.005	1.34
2020-07-06	59036	0.131 ± 0.002	3779.85 ± 292.15	1.660 ± 0.004	1.43
2021-06-09	59374	0.146 ± 0.002	1979.40 ± 151.85	1.665 ± 0.006	1.44
2022-06-28	59758	0.134 ± 0.002	3382.95 ± 275.60	1.682 ± 0.005	1.55
2024-01-07	60316	0.129 ± 0.004	1917.43 ± 283.80	1.630 ± 0.005	1.21

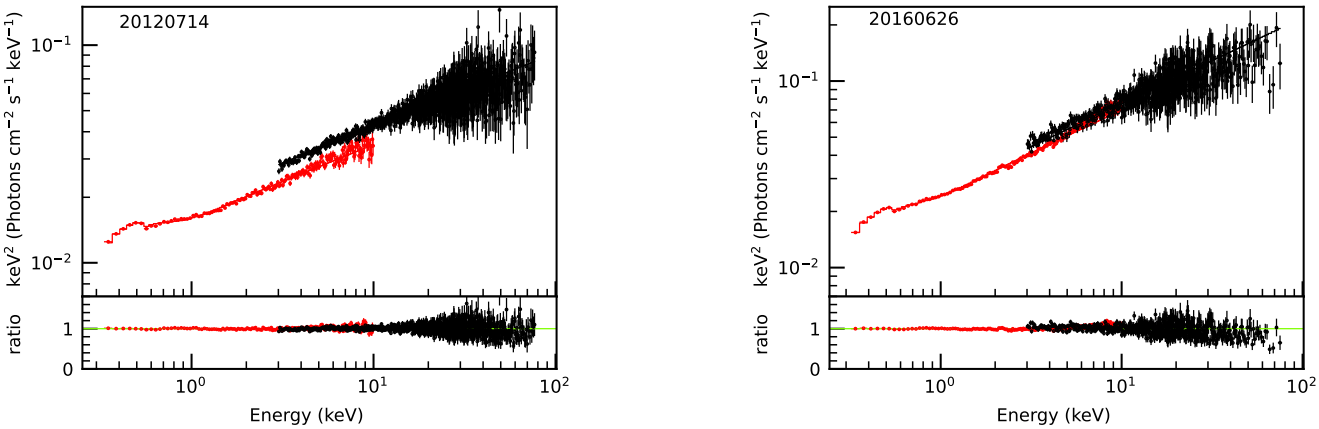

Fig. 2. Sample plots showing TBABS(DISKBB+PL)-fitted 0.3–78 keV spectra of 3C 273 (top panel) and the ratio of data/model (bottom panel). The observation date (yyyymmdd) is mentioned in each plot. Plots for the remaining simultaneous observations are shown in Fig. C.1.

for all the spectra. We illustrate this by plotting the TBABS(PL) model fit to the data and the ratio of the data/model for each spectrum in Fig. 1. The ratio plots show a clear presence of soft excess below 1.5 keV, which indicates a Seyfert-like feature.

We then fitted joint *XMM-Newton* and *NuSTAR* X-ray spectra in the full energy range (0.3–78.0 keV) using the TBABS(DISKBB+PL), model. The fitting results are given in Table 1. The data fitted using this model combination, shown in Fig. 2, returned rather poor fits for all epochs except on MJD 56122. Using the standard relation between DISKBB model normalization and the inner edge of the disc ($R_{\rm in}$), one can determine the colour-corrected inner disc radius (Kubota et al. 1998): $R_{\rm in} = [(D/10\,{\rm kpc})^2\,{\rm Norm_{diskbb}}/\cos i]^{1/2}\kappa^2$ km, where D, i, $\rm Norm_{diskbb}$, and κ are the source distance, disc inclination, normalization for the DISKBB component, and the colour correction factor, respectively. For the values of D ~ 750 Mpc and $i \sim 60^\circ$ (Kriss et al. 1999), $\rm M_{BH} \sim 8 \times 10^8\,M_\odot$ (from this work, see below), $\kappa = 1.6$, and the maximum $\rm Norm_{diskbb}$ value (~3780) estimated on MJD 59036 yield $R_{\rm in} \lesssim 1.7 \times 10^6$ km ~ 0.07 r_S. Such a low $R_{\rm in}$ indicates that the inner disc

Table 2. Best-fitting TBABS*JeTCAF model parameters for all observations of 3C 273.

OBS date.	MJD	M_{BH} ($\times 10^8\ M_\odot$)	$\dot{m}_d$ ($\dot{m}_{Edd}$)	$\dot{m}_h$ ($\dot{m}_{Edd}$)	X_s (r_S)	R	f_{col}	χ^2_r	F_{jet}	F_{corona}
2012-07-13	56121	7.6 ± 1.2	0.010 ± 0.002	0.62 ± 0.05	21.1 ± 2.9	1.69 ± 0.16	0.12 ± 0.03	1.0	2.24 ± 0.07	0.32 ± 0.01
2012-07-14	56122	7.8 ± 1.0	0.015 ± 0.001	0.71 ± 0.04	20.2 ± 2.4	2.18 ± 0.19	0.18 ± 0.01	1.0	2.33 ± 0.12	0.20 ± 0.01
2015-07-13	57216	7.3 ± 0.9	0.016 ± 0.002	0.68 ± 0.04	23.8 ± 2.6	1.89 ± 0.21	0.25 ± 0.04	1.2	1.67 ± 0.11	0.15 ± 0.01
2016-06-26	57565	7.3 ± 1.0	0.020 ± 0.003	0.86 ± 0.06	21.7 ± 2.9	3.75 ± 0.33	0.07 ± 0.02	1.3	3.80 ± 0.11	0.73 ± 0.02
2017-06-26	57930	8.1 ± 1.1	0.022 ± 0.003	0.36 ± 0.01	8.5 ± 1.0	2.17 ± 0.17	0.006 ± 0.001	1.1	1.74 ± 0.05	0.69 ± 0.02
2018-05-19	58257	8.0 ± 1.6	0.014 ± 0.001	0.77 ± 0.04	25.1 ± 2.6	2.65 ± 0.15	0.17 ± 0.02	1.1	1.68 ± 0.04	0.46 ± 0.01
2018-06-02	58271	8.1 ± 1.5	0.016 ± 0.003	0.79 ± 0.04	28.6 ± 2.4	2.64 ± 0.22	0.17 ± 0.02	1.1	1.45 ± 0.03	0.94 ± 0.02
2018-06-15	58284	8.0 ± 1.4	0.018 ± 0.002	0.78 ± 0.03	24.6 ± 2.7	2.56 ± 0.21	0.15 ± 0.01	1.0	1.30 ± 0.03	0.41 ± 0.01
2018-07-04	58303	7.8 ± 1.1	0.016 ± 0.001	0.76 ± 0.02	14.0 ± 1.3	2.86 ± 0.23	0.13 ± 0.02	1.0	1.50 ± 0.06	0.24 ± 0.01
2019-07-02	58666	8.1 ± 1.2	0.020 ± 0.002	0.79 ± 0.03	19.4 ± 2.1	3.24 ± 0.24	0.06 ± 0.01	1.1	1.24 ± 0.04	0.35 ± 0.01
2020-07-06	59036	7.2 ± 1.0	0.020 ± 0.002	0.80 ± 0.04	20.9 ± 2.0	3.36 ± 0.28	0.06 ± 0.01	1.1	1.62 ± 0.04	0.40 ± 0.01
2021-04-14	59318	8.1 ± 1.4	0.013 ± 0.001	0.71 ± 0.02	19.6 ± 2.1	1.90 ± 0.11	0.35 ± 0.05	1.1	0.17 ± 0.00	1.39 ± 0.01
2021-06-09	59374	8.1 ± 1.3	0.018 ± 0.001	0.80 ± 0.02	20.0 ± 2.3	3.17 ± 0.22	0.04 ± 0.01	1.1	1.06 ± 0.03	0.44 ± 0.01
2022-06-28	59758	8.1 ± 1.4	0.020 ± 0.003	0.81 ± 0.02	19.8 ± 2.5	3.10 ± 0.29	0.10 ± 0.02	1.1	1.24 ± 0.03	0.38 ± 0.01
2023-04-12	60046	7.9 ± 0.9	0.017 ± 0.003	0.76 ± 0.03	23.9 ± 2.6	4.69 ± 0.53	0.03 ± 0.01	1.1	–	1.45 ± 0.01
2024-01-07	60316	8.1 ± 1.1	0.020 ± 0.001	0.82 ± 0.01	19.8 ± 2.4	3.30 ± 0.20	0.08 ± 0.02	1.0	1.15 ± 0.03	0.49 ± 0.01

Notes. Epochs with simultaneous *XMM-Newton* observations showed excesses below ~1.5 keV, which required one Gaussian component between energies 0.2–0.5 keV of width 0.1–0.4 keV and another component at ≲0.1 keV of width ~0.4 keV. The fluxes for the jet (F_{jet}) and the corona (F_{corona}) are in units of 10^{-10} erg cm^{-2} s^{-1}. Here '–' in F_{jet} denotes the lowest normalization epoch, where the total flux is taken to be the coronal flux.

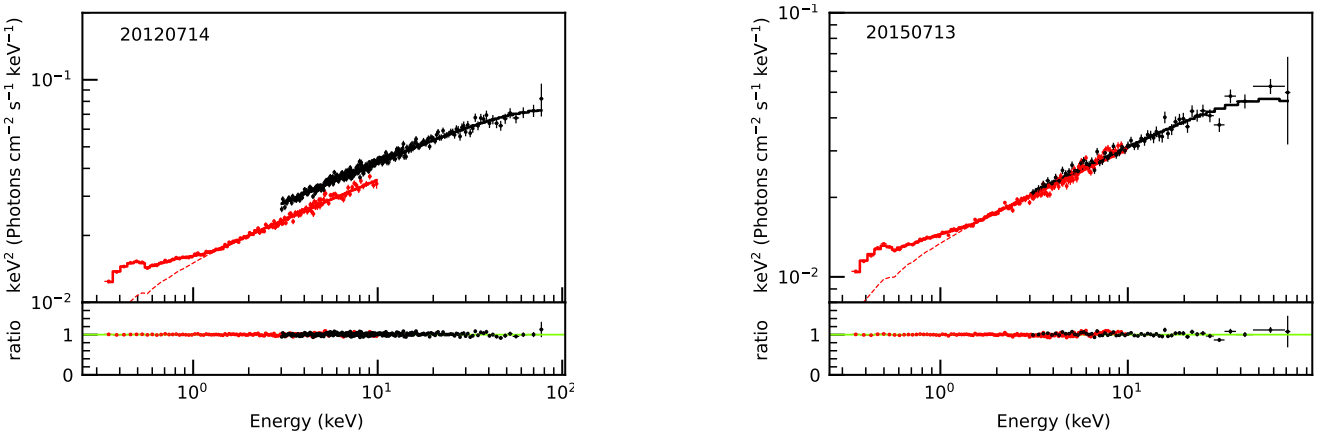

Fig. 3. Sample plots showing JeTCAF-model-fitted 0.3–78.0 keV spectra of 3C 273 (top panel) and the ratio of the data/model (bottom panel). The observation date (yyyymmdd) is mentioned in each plot. Best-fit spectra were rebinned for visual clarity. Plots for the remaining observations are shown in Fig. D.1.

extended well within the innermost stable circular orbit (ISCO), which is non-physical. While we can get estimates of the accretion disc temperature, T_{in} , and spectral slope of the coronal emission, those quantities are the end product of underlying fundamental physical quantities, that is, the mass accretion rate (Shakura & Sunyaev 1973; Sunyaev & Titarchuk 1980; Chakrabarti & Titarchuk 1995). Since the origin of soft X-ray excess is as yet unclear, we also tested a model with two GAUSSIAN components combined with a PL. However, the fit is still not satisfactory ($\chi^2_r > 1.4$). The unsatisfactory results of these model fits motivated us to use an accretion-ejection-based JeTCAF model, which was recently developed by Mondal & Chakrabarti (2021).

We next performed a broad-band (0.3–78.0 keV) X-ray spectral fitting of 3C 273 using simultaneous *XMM-Newton* and *NuSTAR* observations with the JeTCAF model. The JeTCAF-model-fitted parameters are shown in Table 2. Along with JeTCAF model, two GAUSSIAN components were also included to take into account the soft excess below the ~1.5 keV energy range. One component is required between energies 0.2–0.5 keV of width 0.1–0.4 keV and another component at ≲0.1 keV of width ~0.4 keV. Some representative best fits are shown in Fig. 3. The remaining observations are shown in Fig. D.1. When used in XSPEC, the JeTCAF model incorporates the total spectrum, including all components, to fit the observed data. Consequently, the unfolded spectra do not display individual components. However, in theoretical spectra, the individual components can be separated, as demonstrated by Mondal & Chakrabarti (2021).

The variation in model-fitted parameters with observations is shown in Fig. 4. During the combined model fitting, we used BH mass (M_{BH}) as a parameter and kept it free from epoch to epoch. The M_{BH} parameter varies between $(7.2–8.1) \times 10^8\ M_\odot$ and the resulting error-weighted average value is $(7.8 \pm 0.3) \times 10^8\ M_\odot$.

Different estimates of the BH mass of 3C 273 span a broad range of values that were obtained using various methods. Using the reverberation mapping (RM) technique, Laor (1998) estimated a BH mass of $7.4 \times 10^8\ M_\odot$. Kriss et al. (1999) applied

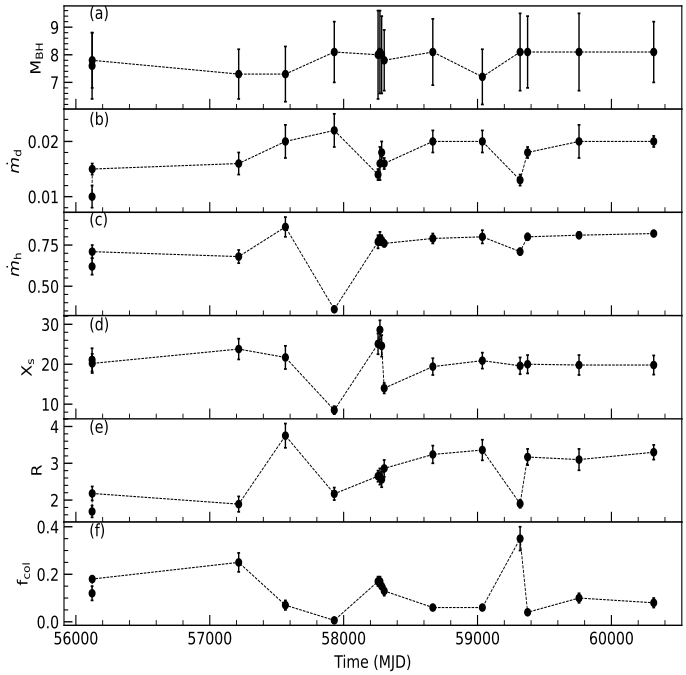

Fig. 4. Temporal variation of best-fitting JeTCAF model parameters: (a) BH mass, (b) disc accretion rate, (c) halo accretion rate, (d) size of the corona, (e) shock compression ratio, and (f) jet collimation factor.

the accretion disc models to broad-band (UV to X-ray) data of 3C 273 to get $M_{\rm BH}$ in a range $(7.1–12)\times10^8\,M_\odot$. Kaspi et al. (2000) calculated a BH mass of $2.35^{+0.37}_{-0.33}\times10^8\,M_\odot$ from the RMS spectra and $5.50^{+0.89}_{-0.79}\times10^8\,M_\odot$ from average spectra using RM of Balmer lines. Paltani & Türler (2005) obtained a substantially higher value of $M_{\rm BH} = 6.6^{+1.6}_{-0.9}\times10^9\,M_\odot$ using RM of broad UV (Lyα and C *IV*) lines. A BH mass of only $2.6\pm1.1\times10^8\,M_\odot$ was measured using the GRAVITY observations (GRAVITY Collaboration 2018). In a recent study, Zhang et al. (2019) estimated a BH mass of $4.1^{+0.3}_{-0.4}\times10^8\,M_\odot$ using a Hβ RM campaign carried out from 2008 to 2018. Our $M_{\rm BH}$ value lies within this range.

Among the other JeTCAF model parameters, the disc mass accretion rate ($\dot{m}_{\rm d}$) varies between 0.010 ± 0.002 to 0.022 ± 0.003 $\dot{m}_{\rm Edd}$, where $\dot{m}_{\rm Edd}$ is the Eddington accretion rate. However, the halo, or sub-Keplerian rate ($\dot{m}_{\rm h}$), varies between 0.36 ± 0.01 to 0.86 ± 0.06 $\dot{m}_{\rm Edd}$, with its value always being higher than $\dot{m}_{\rm d}$. This implies that the spectra are dominated by the hot flow, which indicates that it is hard in nature. As both the mass accretion rates vary from epoch to epoch, the size of the dynamic corona (X_s) also changes significantly from 8.5 ± 1.0 to 28.6 ± 2.4 r_S. It is worth noting that, during MJD 57930, both X_s and $\dot{m}_{\rm h}$ were at minima while $\dot{m}_{\rm d}$ was at its maximum. Such a negative correlation is expected in the JeTCAF framework as the increased accretion rate increases the cooling of the corona and therefore the shock moves inwards (Chakrabarti & Titarchuk 1995; Mondal & Chakrabarti 2013).

The shock compression ratio (R), the ratio of the velocity of the flow inside the corona to that outside the corona, also changes significantly, from 1.9 ± 0.2 to 3.8 ± 0.3. The jet collimation factor ($f_{\rm col}$) variation ranges from a well-collimated outflow (the lowest value: 0.006) to almost a wind-like outflow (the highest value: 0.35). When $\dot{m}_{\rm d}$ is high and $f_{\rm col}$ is near a minimum, we can understand why the outflow is weakest: a cooler corona may not have enough pressure to drive the outflow (Chakrabarti 1999).

Overall, the data fitted this model quite well, which returned reduced $\chi^2\simeq1-1.1$ except for MJDs 57216 and 57565. The best JeTCAF model fits to the 0.3–78.0 keV spectra of 3C 273, as well as the ratios of the data/model check use of '/', are shown in Fig. 3. The best-fitted spectra were rebinned for visual clarity, which does not affect the fitted parameters. After achieving the best fit, we estimated the corona flux ($F_{\rm corona}$) and jet flux ($F_{\rm jet}$) using the lowest model normalization method (see Jana et al. 2017; Mondal et al. 2022a). The best-fitting model gives the total flux ($F_{\rm total}$) and, after replacing the best-fitted model norm by the lowest value obtained from MJD 60046 for this source, this gives the $F_{\rm corona}$. Subtracting $F_{\rm corona}$ from $F_{\rm total}$ yields $F_{\rm jet}$. Therefore, on MJD 60046 there is essentially no jet contribution. On this observation date, the R parameter was maximal (~5), yielding a much lower outflow rate (which is only a function of R), and therefore a much lower flux, which is consistent with the observed spectrum. All JeTCAF model parameters and their variation with MJD are shown in Fig. 4. We note that the JeTCAF model includes the base of the jet, extending from above the corona up to the sonic surface; however, large-scale highly collimated jets (Marshall et al. 2001) cannot be taken into account using this model. The radius of the sonic surface is estimated using the relation $r_c = f_0 X_s/2$ (Chakrabarti 1999), where $f_0 = R^2/R - 1$, which yields $r_c \sim 2.5\times X_s$ (in r_S) for the strong shock case.

In γ-rays, 3C 273 evinces a blazer-like beamed emission component produced by the relativistic jets, so some of the flux is Doppler boosted. Such emission would include photons produced in the jet by the inverse Compton process of thermal and synchrotron X-ray photons from the disc and corona. The present version of the JeTCAF model does not include relativistic beaming effects, and the $F_{\rm jet}$ is calculated as the total jet flux, which may include contributions from other physical processes. The estimated $F_{\rm jet}$ is significantly higher than $F_{\rm corona}$ in almost all epochs. Grandi & Palumbo (2004) reported quite similar results while comparing the jet flux with the Seyfert (non-jetted) type flux using reflection-based models. Moreover, previous estimates of $F_{\rm jet}$ in other jetted sources also showed that $F_{\rm jet}$ is moderately higher or comparable to $F_{\rm corona}$ when the jet was active or moderately weak, respectively, using the TCAF model (Jana et al. 2017; Mondal et al. 2022a). However, for the present source, the jet flux was always higher, which could be due to the effect of Doppler boosting. In such a case, the estimated flux can be used as a tool to estimate the Doppler boosting factor δ (as discussed in Britzen et al. 2007; Hovatta et al. 2009). Assuming that the lowest jet flux, which was observed on MJD 59318, is the base flux and any excess above that is due to the Doppler boosting δ^4. Then the minimum and maximum δ estimated for MJD 59374 and 57565 are 1.6 and 2.2, respectively. This also explains the anti-correlation between $f_{\rm col}$ and $F_{\rm jet}$. Our estimated δ is in agreement with the lowest limit reported by Abraham & Romero (1999).

As a further consistency check of the analysis method and to verify the jet signature in the observed spectra, we redid the fitting using only the TCAF model. For all epochs where only *NuSTAR* data are available, TCAF returned good fits that are similar to JeTCAF-model-fitted statistics. The joint broad-band spectral fitting with TCAF along with GAUSSIAN components for soft-excess also returns satisfactory fits, although with marginally higher fit statistics compared to the JeTCAF, $\Delta\chi^2_r \gtrsim 0.1$. The improvement in fit statistics is due to the presence of two additional components in JeTCAF: (1) some excess at the shoulder of the blackbody (~2–5 keV); and (2) excess above ~50 keV. Keeping in mind that 3C 273 is a 'jetted source', we compared

the parameters of both models and find that the TCAF model fits require a higher $\dot{m}_d$ and R for all epochs. Noticeably, the R values obtained from TCAF fits are high, falling in the >4 range. However, in the TCAF scenario, jets or outflows are significant and are launched for intermediate values of R (∼2−3; Chakrabarti 1999) and when the disc accretion rate is low. These are closely consistent with JeTCAF- model-fitted parameters. The $\dot{m}_h$ and X_s obtained from both models are nearly similar. This comparison shows that the contribution of the jet to the observed spectra is robust in the model fitting.

4. Conclusions

The extremely bright nearby quasar 3C 273 has shown properties typical of both jetted-AGNs and Seyfert galaxies, which makes it a perfect source for examining the disc-jet interactions in AGNs. In this work, we fitted the broad-band (0.3–78.0 keV) X-ray data of 3C 273 from *XMM-Newton* and *NuSTAR* using combined accretion-ejection and jet-based models. We summarize the main findings of our investigation below:

- A simple PL fit left significant X-ray excess at energies below ∼1.5 keV, which suggests emission from the accretion disc-corona system.
- The accretion disc model that was added to the PL did not yield an acceptable fit.
- The accretion-ejection-based JeTCAF model provided the best fits along with sensible accretion flow parameters.
- The value of the model parameter M_{BH} remains consistent for all the observations. The weighted-mean value of M_{BH} is $(7.77 \pm 0.30) \times 10^8\ M_\odot$, which falls in the range of M_{BH} values estimated using RM and other accretion-based models in the literature.
- A broad range in the f_{col} parameter indicates the presence of both collimated and wind-like outflows from the system.
- For all observations $\dot{m}_h > \dot{m}_d$ and X_s were relatively high, a combination associated with the hard spectra from the corona region, and consistent with the PL-model-fitted Γ, <1.8.
- If the estimated jet flux is used to estimate the Doppler boosting factor, we obtain values between 1.6–2.2, which are consistent with the lowest value found in the literature.

Acknowledgements. We sincerely thank the referee for their insightful comments and suggestions. The project was partially supported by the Polish Funding Agency National Science Centre, project 2017/26/A/ST9/00756 (MAESTRO 9). AP acknowledges funding from the Chinese Academy of Sciences President's International Fellowship Initiative (PIFI), Grant No. 2024PVC0088. SM acknowledges the Ramanujan Fellowship (RJF/2020/000113) by DST-SERB, Govt. of India for this research.

References

Abdo, A. A., Ackermann, M., Ajello, M., et al. 2010, ApJ, 714, L73
Abraham, Z., & Romero, G. E. 1999, A&A, 344, 61
Blandford, R. D., & Payne, D. G. 1982, MNRAS, 199, 883
Blandford, R. D., & Znajek, R. L. 1977, MNRAS, 179, 433
Blandford, R., Meier, D., & Readhead, A. 2019, ARA&A, 57, 467
Britzen, S., Brinkmann, W., Campbell, R. M., et al. 2007, A&A, 476, 759
Chakrabarti, S. K. 1989, ApJ, 347, 365
Chakrabarti, S. K. 1999, A&A, 351, 185
Chakrabarti, S., & Titarchuk, L. G. 1995, ApJ, 455, 623
Chernyakova, M., Neronov, A., Courvoisier, T. J. L., et al. 2007, A&A, 465, 147
Chidiac, C., Rani, B., Krichbaum, T. P., et al. 2016, A&A, 590, A61
Das, S., & Chatterjee, R. 2023, MNRAS, 524, 3797
Debnath, D., Chakrabarti, S. K., & Mondal, S. 2014, MNRAS, 440, L121
Fan, J. H., Peng, Q. S., Tao, J., Qian, B. C., & Shen, Z. Q. 2009, AJ, 138, 1428
Fan, J. H., Kurtanidze, O., Liu, Y., et al. 2014, ApJS, 213, 26
Fernandes, S., Patiño-Álvarez, V. M., Chavushyan, V., Schlegel, E. M., & Valdés, J. R. 2020, MNRAS, 497, 2066
Ghisellini, G., Tavecchio, F., Foschini, L., & Ghirlanda, G. 2011, MNRAS, 414, 2674
Grandi, P., & Palumbo, G. G. C. 2004, Science, 306, 998
GRAVITY Collaboration (Sturm, E., et al.) 2018, Nature, 563, 657
HI4PI Collaboration (Ben Bekhti, N., et al.) 2016, A&A, 594, A116
Hovatta, T., Valtaoja, E., Tornikoski, M., & Lähteenmäki, A. 2009, A&A, 494, 527
Hutsemékers, D., Borguet, B., Sluse, D., & Pelgrims, V. 2018, A&A, 620, A68
Jana, A., Chakrabarti, S. K., & Debnath, D. 2017, ApJ, 850, 91
Kalita, N., Gupta, A. C., Wiita, P. J., Bhagwan, J., & Duorah, K. 2015, MNRAS, 451, 1356
Kaspi, S., Smith, P. S., Netzer, H., et al. 2000, ApJ, 533, 631
Kataoka, J., Tanihata, C., Kawai, N., et al. 2002, MNRAS, 336, 932
Kriss, G. A., Davidsen, A. F., Zheng, W., & Lee, G. 1999, ApJ, 527, 683
Kubota, A., Tanaka, Y., Makishima, K., et al. 1998, PASJ, 50, 667
Laor, A. 1998, ApJ, 505, L83
Livio, M., Pringle, J. E., & King, A. R. 2003, ApJ, 593, 184
Madsen, K. K., Fürst, F., Walton, D. J., et al. 2015, ApJ, 812, 14
Maraschi, L., & Tavecchio, F. 2003, ApJ, 593, 667
Marshall, H. L., Harris, D. E., Grimes, J. P., et al. 2001, ApJ, 549, L167
Molla, A. A., Chakrabarti, S. K., Debnath, D., & Mondal, S. 2017, ApJ, 834, 88
Mondal, S., & Chakrabarti, S. K. 2013, MNRAS, 431, 2716
Mondal, S., & Chakrabarti, S. K. 2021, ApJ, 920, 41
Mondal, S., Rani, P., Stalin, C. S., Chakrabarti, S. K., & Rakshit, S. 2022a, A&A, 663, A178
Mondal, S., Adhikari, T. P., Hryniewicz, K., Stalin, C. S., & Pandey, A. 2022b, A&A, 662, A77
Mukherjee, S., Mitra, K., & Chatterjee, R. 2019, MNRAS, 486, 1672
Padovani, P., Alexander, D. M., Assef, R. J., et al. 2017, A&ARv, 25, 2
Paltani, S., & Türler, M. 2005, A&A, 435, 811
Paltani, S., Courvoisier, T. J. L., & Walter, R. 1998, A&A, 340, 47
Rees, M. J. 1984, ARA&A, 22, 471
Sambruna, R. M., Urry, C. M., Tavecchio, F., et al. 2001, ApJ, 549, L161
Sbarrato, T., Padovani, P., & Ghisellini, G. 2014, MNRAS, 445, 81
Schmidt, M. 1963, Nature, 197, 1040
Shakura, N. I., & Sunyaev, R. A. 1973, A&A, 500, 33
Soldi, S., Türler, M., Paltani, S., et al. 2008, A&A, 486, 411
Stocke, J. T., Morris, S. L., Gioia, I. M., et al. 1991, ApJS, 76, 813
Sunyaev, R. A., & Titarchuk, L. G. 1980, A&A, 500, 167
Türler, M., Courvoisier, T. J. L., & Paltani, S. 2000, A&A, 361, 850
Valtaoja, L., Takalo, L. O., Sillanpaa, A., et al. 1991, AJ, 102, 1946
Walter, R., & Courvoisier, T. J. L. 1992, A&A, 258, 255
Wandel, A., & Urry, C. M. 1991, ApJ, 367, 78
Xie, G. Z., Li, K. H., Zhang, X., Bai, J. M., & Liu, W. W. 1999, ApJ, 522, 846
Zdziarski, A. A., & Grandi, P. 2001, ApJ, 551, 186
Zhang, Z.-X., Du, P., Smith, P. S., et al. 2019, ApJ, 876, 49

Appendix A: Observation log

Table A.1. Log of simultaneous *NuSTAR* and *XMM-Newton* observations.

NuSTAR			*XMM-Newton*		
ObsID	Observation start date and time	Exposure (ks)	ObsID	Observation start date and time	Exposure (ks)
10012004001	2012-07-13 11:11:07	6.23	-	-	-
10002020001	2012-07-14 00:06:07	243.97	0414191001	2012-07-16 11:59:23	38.92
10002020003	2015-07-13 14:01:08	49.41	0414191101	2015-07-13 21:03:55	72.40
10202020002	2016-06-26 19:11:08	35.41	0414191201	2016-06-26 20:22:08	67.20
10302020002	2017-06-26 17:41:09	35.40	0414191301	2017-06-26 19:15:23	67.00
80301602002	2018-05-19 18:01:09	60.76	-	-	-
10402020002	2018-06-02 02:01:09	16.09	-	-	-
10402020004	2018-06-15 04:31:09	21.18	-	-	-
10402020006	2018-07-04 17:21:09	40.32	0414191401	2018-07-04 17:54:16	78.00
10502620002	2019-07-02 07:51:09	49.41	0810820101	2019-07-02 17:16:32	69.40
10602606002	2020-07-06 04:56:09	44.02	0810821501	2020-07-06 11:59:20	69.90
60601004002	2021-04-14 14:46:09	18.67	-	-	-
10702608002	2021-06-09 18:36:09	36.04	0810821601	2021-06-09 19:26:58	65.00
10802608002	2022-06-28 01:11:09	33.18	0810821901	2022-06-28 02:36:00	61.80
60701019002	2023-04-12 17:16:09	19.75	-	-	-
11002608002	2024-01-07 11:16:09	43.03	0810822101	2024-01-07 16:43:21	62.99

Appendix B: Plots showing PL fitting to 0.3-10 keV spectra of 3C 373

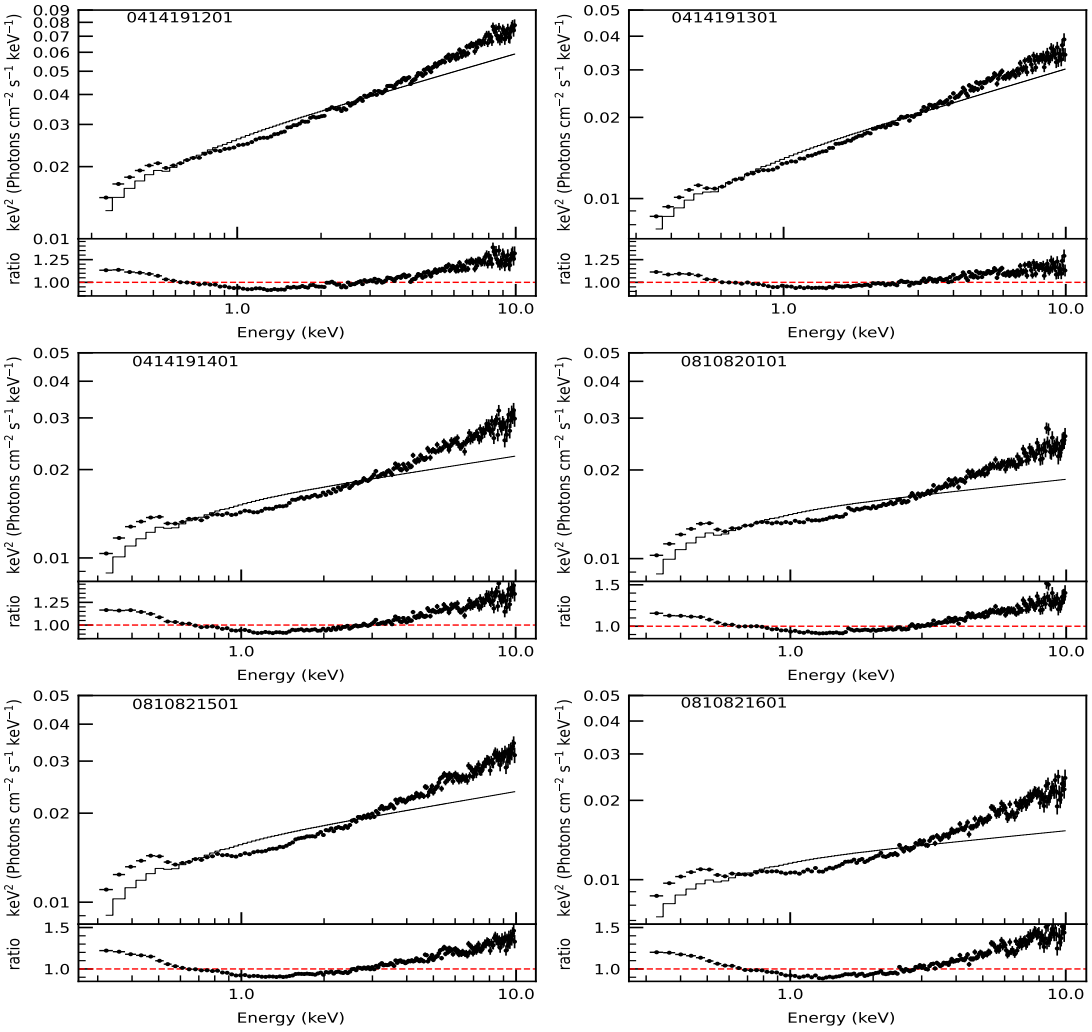

Fig. B.1. Simple PL fitted 0.3-10 keV spectra of 3C 273. The ratio of data/model is plotted in the bottom portion of each panel.

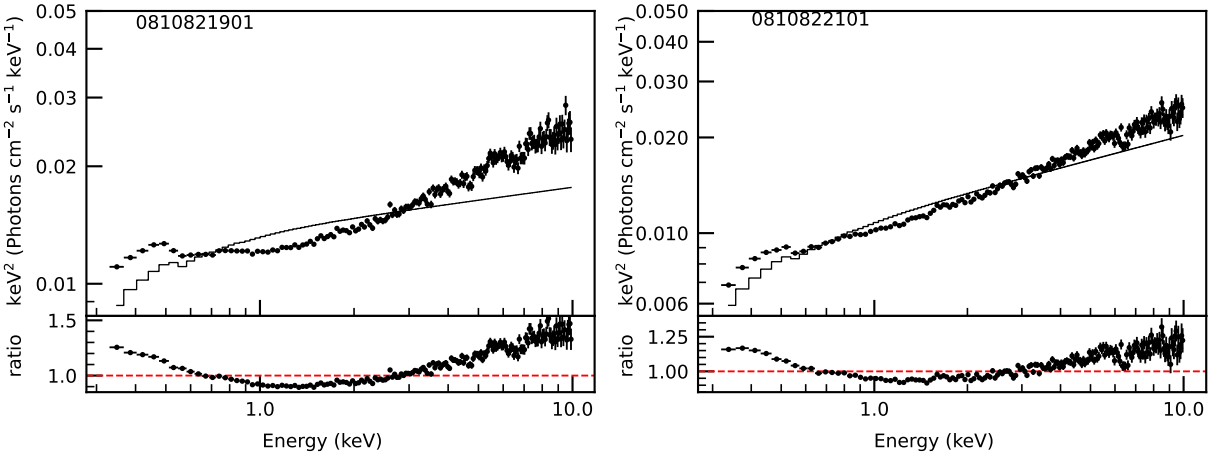

Fig. B.1. Continued.

Appendix C: Plots showing TBABS(DISKBB+PL) fitting to 0.3-78 keV spectra of 3C 273

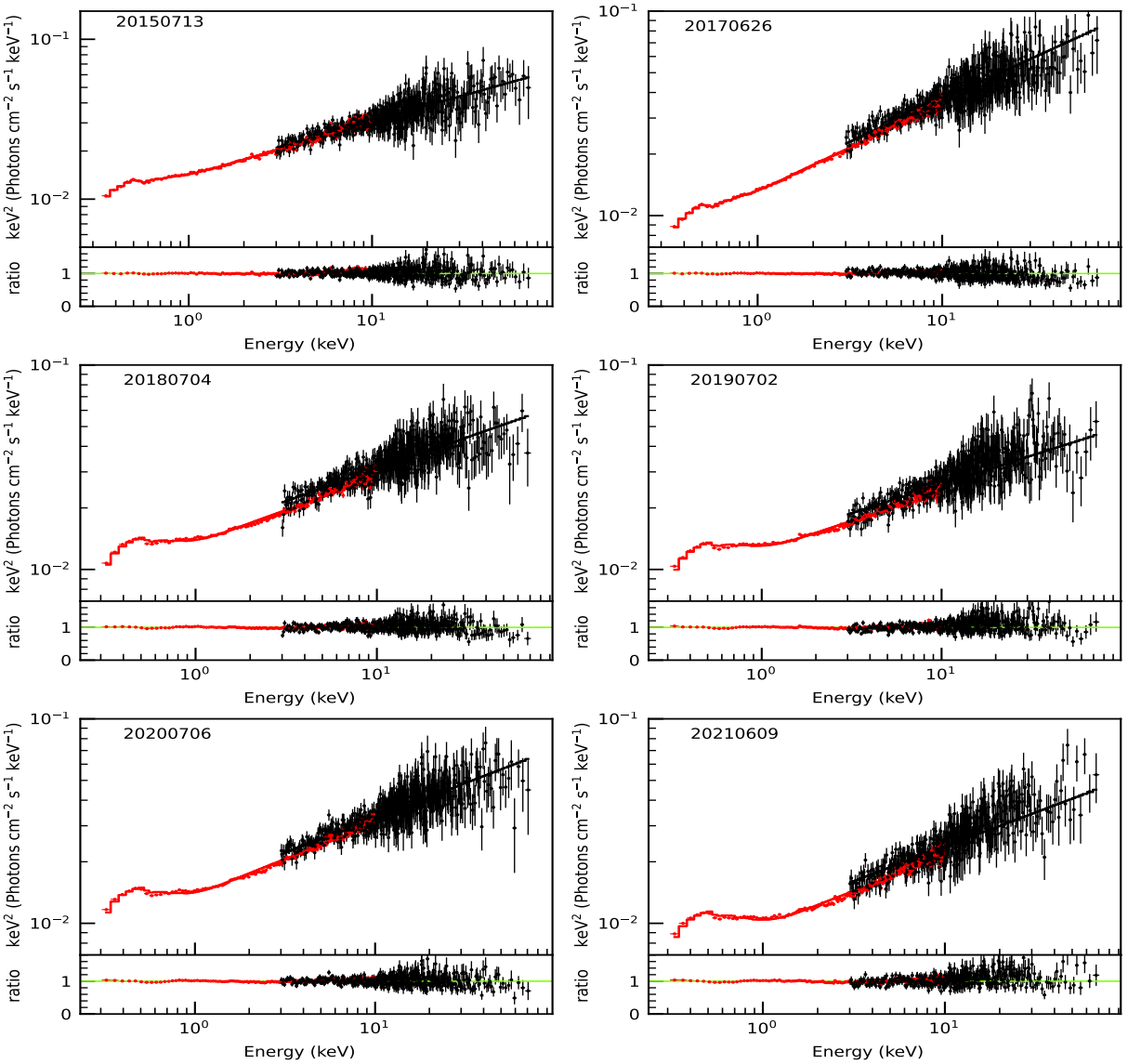

Fig. C.1. TBABS(DISKBB+PL) model fitted 0.3-78 keV spectra of 3C 273. The ratio of data/model is plotted in the bottom portion of each panel.

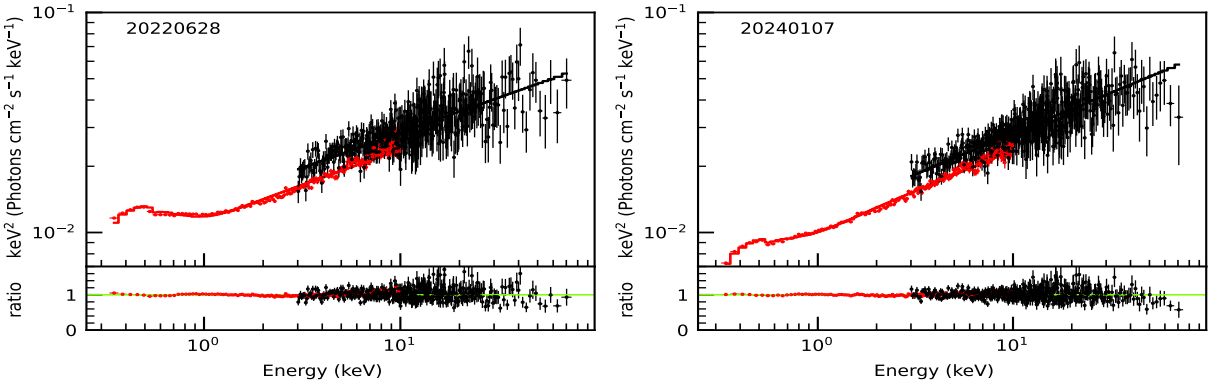

Fig. C.1. Continued.

Appendix D: Plots showing the JeTCAF model fitted 0.3-78.0 keV spectra of 3C 273

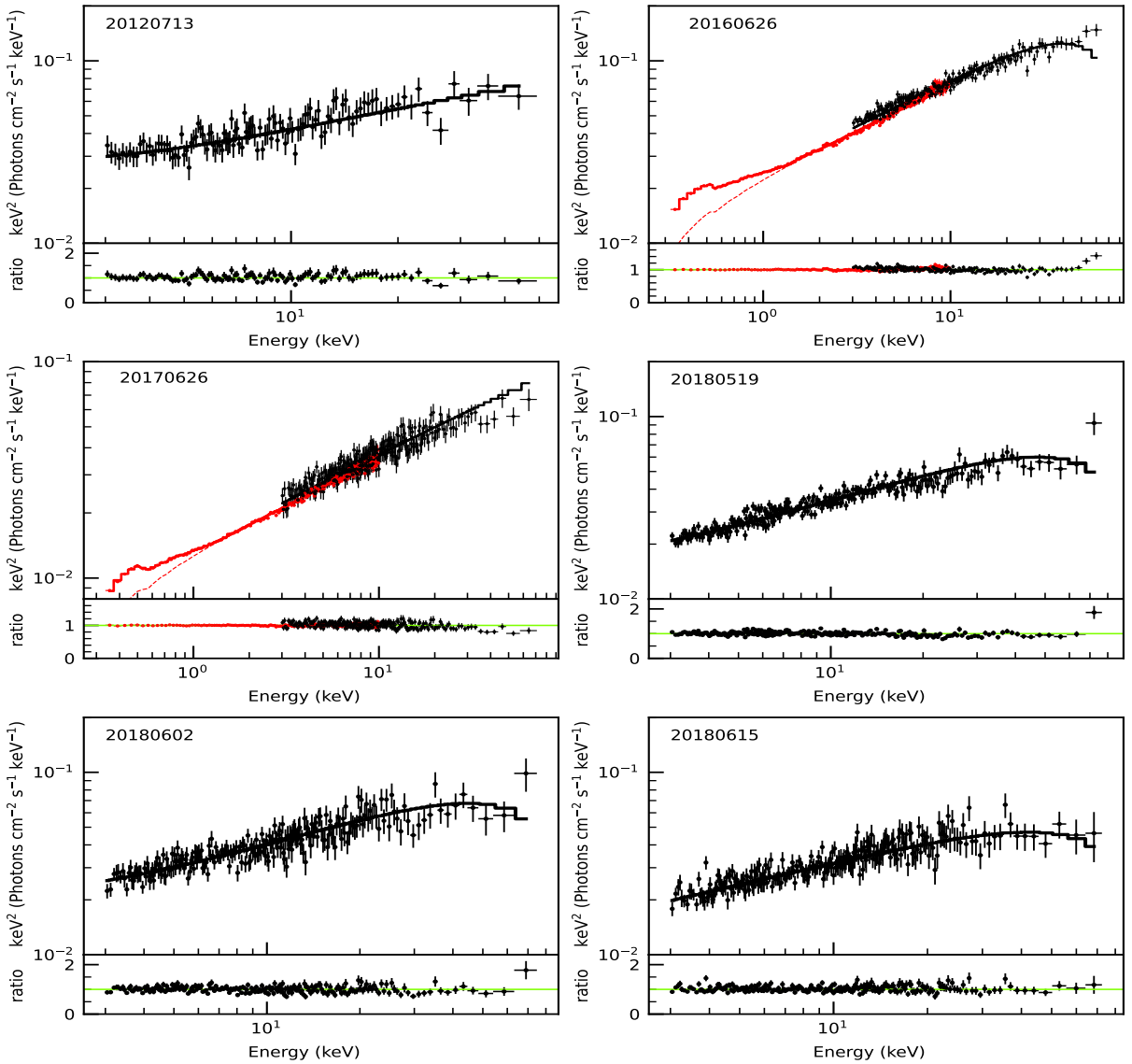

Fig. D.1. JeTCAF model fitted 0.3−78.0 keV spectra of 3C 273. The ratio of data/model is plotted in the bottom portion of each panel.

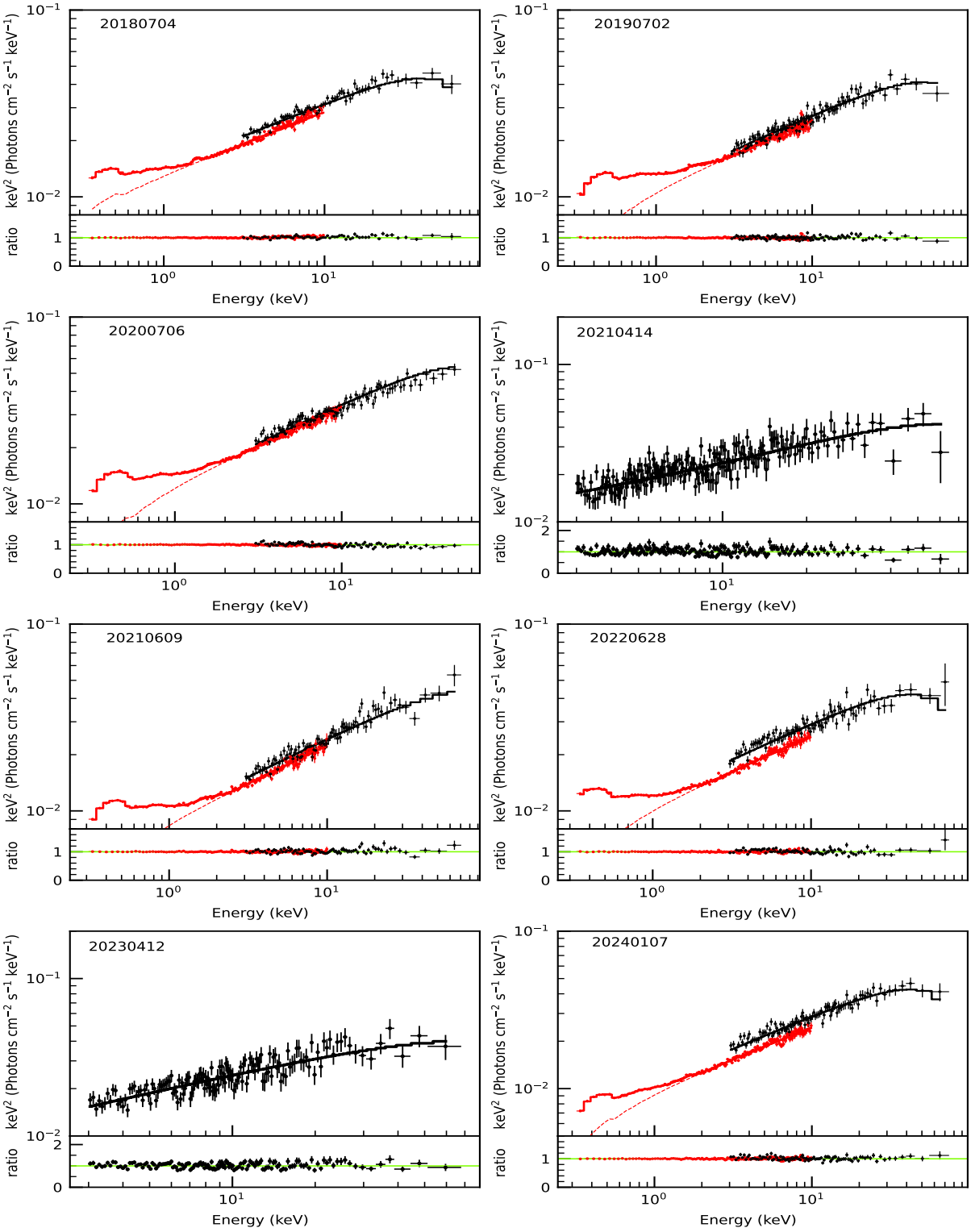

Fig. D.1. Continued.